Published in final edited form as:

Cell Rep. 2021 July 06; 36(1): 109335. doi:10.1016/j.celrep.2021.109335.

A double-negative gene regulatory circuit underlies the virgin behavioral state

Daniel L. Garaulet[1,*], **Albertomaria Moro**[1], **Eric C. Lai**[1,2,*]

[1]Developmental Biology Program, Sloan Kettering Institute, New York, NY 10065, USA

[2]Lead contact

SUMMARY

Virgin females of many species conduct distinctive behaviors, compared with post-mated and/or pregnant individuals. In *Drosophila,* this post-mating switch is initiated by seminal factors, implying that the default female state is virgin. However, we recently showed that loss of miR-iab-4/8-mediated repression of the transcription factor Homothorax (Hth) within the abdominal ventral nerve cord (VNC) causes virgins to execute mated behaviors. Here, we use genomic analysis of *mir-iab-4/8* deletion and hth-microRNA (miRNA) binding site mutants (*hth[BSmut]*) to elucidate *doublesex (dsx)* as a critical downstream factor. Dsx and Hth proteins are highly complementary in CNS, and Dsx is downregulated in *miRNA/hth[BSmut]* mutants. Moreover, virgin behavior is highly dose sensitive to developmental *dsx* function. Strikingly, depletion of Dsx from very restricted abdominal neurons (SAG-1 cells) abrogates female virgin conducts, in favor of mated behaviors. Thus, a double-negative regulatory pathway in the VNC (miR-iab-4/8 ⊣ Hth ⊣ Dsx) specifies the virgin behavioral state.

Graphical abstract

*Correspondence: dlgaraulet@gmail.com (D.L.G.), laie@mskcc.org (E.C.L.).

AUTHOR CONTRIBUTIONS

Conceptualization, D.L.G., E.C.L.; methodology, D.L.G.; formal analysis, D.L.G., A.M.; investigation, D.L.G., A.M., E.C.L.; resources, D.L.G., E.C.L.; visualization, D.L.G.; supervision, D.L.G., E.C.L.; writing - original draft, D.L.G., E.C.L.; writing - review and editing, D.L.G., E.C.L.; project administration, D.L.G., E.C.L.; funding acquisition, E.C.L.

SUPPLEMENTAL INFORMATION

Supplemental information can be found online at https://doi.org/10.1016/j.celrep.2021.109335.

DECLARATION OF INTERESTS

The authors declare no competing interests.

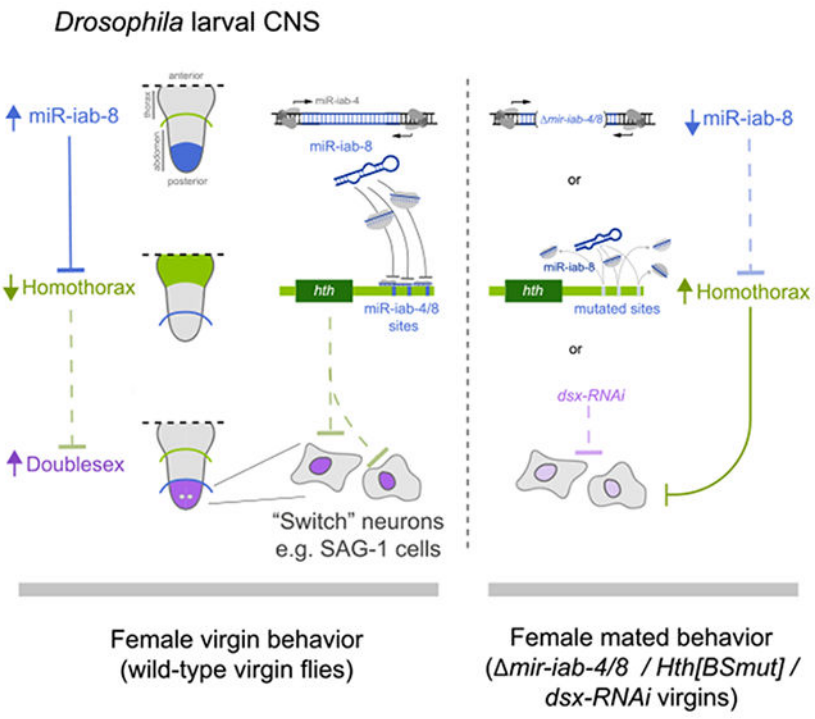

In brief

Garaulet et al. use transcriptomic analysis to reveal new downstream elements in a post-transcriptional cascade, via miR-iab-4/8 and Homothorax, that affects patterning of the CNS. This genetic circuit regulates the accumulation of a secondary target (Doublesex), whose level in specific neurons determines the behavior of adult virgin flies.

INTRODUCTION

Females of diverse invertebrate and vertebrate species coordinate multiple behavioral programs with their reproductive state. Mature female virgins are receptive to male courtship and copulation, but following mating and/or pregnancy, they decrease sexual activity and modulate behaviors to generate and foster their children. Behavioral remodeling associated with the female reproductive state includes increased aggression and nest building in avians and mammals (Ogawa and Makino, 1984; Svare et al., 1982) and decreased male acceptance, increased egg-laying, and appetitive/metabolic changes in insects (Anholt et al., 2020). The genetic and neurological control of this process has been intensively studied in fruit flies, where sexual activity induces the post-mating switch, a host of behavioral changes collectively known as post-mating responses (PMRs) (Anholt et al., 2020).

In *Drosophila,* as in other species, "virgin" is typically considered the default behavioral state, because factors that induce PMRs are transferred in seminal fluids during copulation. Among these, Sex Peptide (SP) is necessary and sufficient to drive most female post-mated behaviors (Kubli and Bopp, 2012). SP signals via uterine SP sensory neurons (SPSNs) (Feng et al., 2014; Häsemeyer et al., 2009; Yang et al., 2009). Some $SPSN^{+}$ neurons contact

abdominal interneurons in the ventral nerve cord (VNC) that express myoinhibitory peptide (Jang et al., 2017), which input into a restricted population of ascending neurons (SP abdominal ganglion [SAG] neurons) that project to the posterior brain, including pC1 neurons (Feng et al., 2014; Soller et al., 2006; Wang et al., 2020b). This outlines an ascending flow of information for how a seminal fluid peptide can alter female brain activity. The brain integrates this with auditory and visual cues to coordinate diverse behaviors mediated by distinct lineages of descending neurons and VNC populations that modulate specific behaviors according to internal state and external stimuli (Mezzera et al., 2020; Wang et al., 2020a, 2020b, 2021).

Recently, we found that post-transcriptional suppression of the homeobox gene *homothorax* (*hth*) within the VNC is critical to implement the virgin behavioral state (Garaulet et al., 2020). Of note, deletion of the Bithorax Complex (BX-C) locus *mir-iab-4/8,* point mutations of their binding sites in *hth,* or deletion of the *hth* neural-specific 3′ UTR extension bearing many of these microRNA (miRNA) sites all cause mutant female virgins to perform mated behaviors. Thus, the failure to integrate two post-transcriptional regulatory inputs at a single target gene prevents females from appropriately integrating their sexual internal state with external behaviors.

Our recognition of the transcription factor Hth as a target of regulatory circuits for virgin behavior implies that downstream loci may serve as a functional output for this process. Here, we used molecular genetic profiling to identify a critical requirement for Doublesex (Dsx) to implement the female virgin behavioral state. Dsx has been well studied with respect to differentiation of sexually dimorphic traits (Kopp, 2012), but its roles in post-mitotic neurons are little known. We find that expression of Dsx in the VNC mediates virgin behavior, and that modulation of Dsx in only a few abdominal VNC neurons is sufficient to convert the suite of female virgin behaviors into mated conducts.

RESULTS

VNC-iab-8 domain transcriptomes of BX-C miRNA and hth-miRNA binding site mutants

The bidirectionally transcribed BX-C miRNA locus encodes distinct miRNAs, *mir-iab-4* and *mir-iab-8*, which are expressed in adjacent Hox-like patterns along the embryonic anterior-posterior axis. GFP sensors and *in situ* hybridization reveal these miRNAs are active in adjacent domains of the abdominal VNC from embryo to adult, with miR-iab-8 deployed in segments posterior to A7 (Bender, 2008; Garaulet et al., 2014; Gummalla et al., 2012; Tyler et al., 2008) Figure 1A, referred hereafter as the iab-8 domain). Expression of the BX-C Hox gene abd-A largely overlaps miR-iab-4 and demarcates the anterior miR-iab-8-5p activity domain (Figure 1B). In flies deleted for *mir-iab-4/8* (trans-heterozygous Δ/*C11* mutants), ectopic Hth proteins accumulate in both miRNA domains from larval stages (Figure 1C) to adult (Garaulet et al., 2014, 2020). Specific mutations of all miR-iab-4/8 binding sites in the 3′ UTR of the homeodomain-encoding isoform of *homothorax* (*hth[BSmut]*) also derepress Hth protein (Figure 1C). Although genetic evidence indicates both miRNAs contribute to the Δ*mir-iab-4/8* phenotype in female virgins, ectopic Hth in *hth[BSmut]* is most overt within the miR-iab-8 domain (Figures 1C and 1H) and is sufficient to induce PMRs in virgin females (Garaulet et al., 2020).

Based on this, we sought to collect transcriptome data from the female iab-8 VNC domain. Because we lack markers that permit positive selection of this region, we opted for manual separation. We analyzed larval VNC, which owing to its more extended morphology than adult VNC, was more amenable to microdissection. With practice, we could reproducibly sever the VNC at the A7 pair of nerves, posterior to the major domain of abd-A as assessed by *post hoc* immunostaining (Figure 1D), thus liberating the iab-8 region of the VNC (segments A8 and A9). We prepared triplicate RNA sequencing (RNA-seq) samples from this region from the three genotypes (Figure 1D; Figure S1).

Although both mutants were reproducibly distinct from *Canton-S* control, they exhibited limited overall changes in gene expression (Figure S1). We queried Δ*mir-iab-4/8* data with respect to different classes of conserved seed matches for miR-iab-8-5p (http://www.targetscan.org/vert_72/). Among genes expressed at a minimum level (>1 RPKM), the strong majority bearing target sites were unchanged (Figure 1E; Figure S1), and only modestly more targets were upregulated than downregulated (at 1.5-fold change, 10 up and 6 down; Figure 1E). Bulk tissue sequencing might underestimate target responses if they were heterogeneous on a cell-by-cell basis. For example, we did not observe significant changes in validated BX-C Hox gene targets *Ubx* and *abd-A* (Tyler et al., 2008) (Figure 1F), which detectably express ectopic, although sporadic, proteins within the iab-8 domain of BX-C miRNA mutants (Bender, 2008; Garaulet et al., 2014; Gummalla et al., 2012). In any case, because the effects of BX-C miRNA deletion on their targets in abdominal VNC were limited, it was notable that two of the highest and most significantly upregulated miR-iab-8-5p targets were *hth* and *extradenticle* (*exd*) (Garaulet et al., 2014) (Figures 1E and 1G). Consistent with detection of ectopic Hth protein, the iab-8 region of *hth [BSmut]* VNC also derepressed *hth* but did not upregulate *exd,* whose levels were changed only in Δ*mir-iab-4/8* (Figure 1G; Figure S1).

Hth and Exd are heterodimeric TALE-homeodomain proteins that act as Hox gene cofactors but also have independent functions. Hth is a spatially patterned nuclear factor, and in the VNC, the anterior boundary of iab-4 activity is normally coincident with the loss of Hth (Figure 1C) (Garaulet et al., 2020). Exd is expressed more broadly but remains cytoplasmic in the absence of Hth, which serves as its nuclear escort (Pai et al., 1998; Rieckhof et al., 1997). Because of this, nuclear Exd is very sparse in wild-type abdominal VNC segments. In contrast, BX-C miRNA mutants broadly exhibit ectopic nuclear Exd within both iab-4 and iab-8 domains (Figure 1H) (Garaulet et al., 2014). If this required joint release of both genes from miRNA control, we might expect a different pattern of abdominal Exd in *hth[BSmut].* However, the nuclear intensity of ectopic Exd colocalized to that of Hth and was similar between the two mutants, despite the fact that *exd* RNA increased only in *mir[Δ/C11]* and not *hth[BSmut]* mutant VNC (Figures 1G and 1H). We quantified the iab-8 domains of the three genotypes of overtly Exd^+ nuclei and observed comparable, strong increases in both *mir[Δ/C11]* and *hth [BSmut]* mutants (Figure 1I). This suggests that even though Exd is a prominent miR-iab-4/8 target (Figure 1E) (Garaulet et al., 2014), it is not limiting for derepressed Hth to exert phenotypic or regulatory effects in these mutants.

Given the restricted effects of BX-C miRNA loss on direct targets in the iab-8 VNC, we examined features of presumably indirect expression changes. If derepressed Hth was

responsible for some of these effects, they might be associated with overlapping responses between miRNA deletion and *hth[BSmut]* VNC. Intriguingly, we observe substantial overlaps between their up- and downregulated gene sets, with relatively few genes exhibiting discordant behavior (Figure 2A; Table S1). Co-regulated loci included neuronal receptors, channels, and peptide hormones (Figure S2). Taken together, these data were consistent with the notion that deregulated Hth may drive aberrant gene expression downstream of BX-C miRNA loss.

Spatial complementarity of Hth and Dsx is disrupted by loss of miRNA regulation

Among genes co-regulated by BX-C miRNA loss and deletion of their binding sites from *hth,* we were particularly intrigued by *doublesex* (*dsx*), which was ~2-fold lower in both mutants (Figures 2A and 2B). This transcription factor is widely studied for its central role in sex determination locus, and its vertebrate homolog DMRT1 similarly controls sex-specific differentiation (Kopp, 2012). However, less is known about its functions in post-mitotic neurons. We were intrigued by the highly spatially complementary pattern of Dsx and Hth proteins in the nervous system. In the VNC, Dsx protein is restricted to the posterior abdominal ganglion and abuts the domain of Hth, located more anteriorly (Figure 2C); very few neurons co-express these proteins (Figure S3). The reciprocal pattern of Dsx and Hth also extends to the brain. Although Dsx accumulates more sparsely in this setting, only rarely is Dsx colocalized with Hth, even among closely apposed cells (Figure S3).

Immunostaining of BX-C miRNA mutants revealed a decrease in Dsx^+ neurons in the abdominal ganglion of both miRNA and *hth[BSmut]* mutants, which was most visually evident in their dorsal regions (Figure 2D). We quantified all Dsx^+ neurons throughout the volume of the VNC and observed ~150 fewer Dsx^+ neurons in both mutant conditions (Figure 2E), but the difference was greater in the dorsal half (Figure 2E). We recently showed that repression of *hth* by BX-C miRNAs that is relevant for female PMRs occurs in specific abdominal VNC neurons, marked by *VT-7068, VT-454,* and *VT-50405* Gal4 drivers (i.e., Vienna Tiles [VT]-switch lines) (Feng et al., 2014; Garaulet et al., 2020). Because the numbers of neurons labeled by these drivers (~80–300) were not substantially affected in miRNA mutants (Figure 2F), loss of Dsx reactivity in mutants was not due to loss of abdominal neurons that mediate the post-mating switch per se.

The regulatory intersection of *VT-7068* and *VT-50405* (as a split-Gal4 combination) labels a handful of neurons in the entire CNS of female flies, with typically four “SAG-1” abdominal neurons found in the iab-8 domain (Figure S4)(Feng et al., 2014). These project to the central brain (Figure S4) and constitute a minimal set of VNC cells whose enforced activation can partially induce virgin behaviors in mated females (Feng et al., 2014). We employed these abdominal SAG-1 neurons for quantitative analysis of Hth and Dsx, taking great care to stain wild-type and mutant VNC in the same wells and to image them in parallel using identical settings (see STAR Methods). We reliably observed elevated Hth in identified SAG-1 neurons, in both miRNA deletion and *hth[BSmut]* mutants, concomitant with downregulation of Dsx (Figures 2G and 2H). Dsx exhibits a moderately bimodal distribution in wild-type SAG-1 neurons (Figures 2G and 2H). However, deletion of BX-C miRNAs eliminates most of the Dsx-high class, and total levels of Dsx are significantly

lower in both *mir-iab-4/8* and *hth[BSmut]* mutants (Figure 2G). Therefore, loss of miRNA-mediated regulation of Hth results in its derepression in abdominal VNC neurons, which in turn is associated with decreased Dsx.

To understand if the decrease in abdominal Dsx protein was promoted by elevated Hth, we misexpressed *hth* in SAG-1 neurons and analyzed Dsx in abdominal SAG-1 nuclei. This reduced Dsx slightly, although the difference with wild-type was not significant (Figure S4). Conversely, ectopic Dsx decreased Hth moderately (Figure S4). However, these experiments are difficult to interpret due to high levels of overexpressed Hth or Dsx, which are likely non-physiological (Figure S4). Therefore, we utilized a different approach to deplete *hth* in *mir-iab-4/8* mutants. In *SAG-1>hth-RNAi; mir[Δ/C11]* virgins, Dsx levels and distribution were restored to wild-type values (Figures 2G and 2H). Thus, the decrease in Dsx proteins in mutants requires elevation of endogenous Hth. In other words, there is a double-negative relationship extending from the miRNA to Hth to Dsx.

Dsx is highly dose sensitive for female virgin behavior

dsx is necessary for male courtship (McRobert and Tompkins, 1985), as well as to specify the female circuitry necessary for the post-mating switch (Rezával et al., 2012; Rideout et al., 2010; Robinett et al., 2010). However, despite the fact that *dsx*-expressing neurons are required for female reproductive behaviors, the function of Dsx in female behavior has received comparably little attention.

We initially examined loss-of-function alleles of *dsx.* Null mutants display inter-sex cuticular features, including male and female elements on their genitalia and sex combs (Nothiger et al., 2009), but *dsx* heterozygotes develop normal genitalia and normal numbers and appearance of sex combs on male forelegs (Figure S5). Thus, a single copy of *dsx* is sufficient for gross anatomy.

We then examined female behavior. The two most commonly monitored aspects of the post-mating switch are egg-laying and receptivity. Female virgins are highly receptive to male courtship and lay few eggs in the first few days after eclosion (Figures 3A and 3B). Following copulation, females become refractory to further copulation attempts for several days and increase egglaying substantially (Anholt et al., 2020) (Figures 3A and 3B). Surprisingly, *dsx* heterozygosity compromises both behaviors: egg-laying is increased and receptivity is decreased compared with wild-type virgins. Importantly, both readouts were similarly affected in independent *dsx* alleles, compared with their control siblings (Figures 3A and 3B). Together, these slight but genetically robust differences in egg-laying and receptivity seemed to indicate a partial transition to the mated state in pre-inseminated virgins, triggered by *dsx* heterozygosity. To confirm this hypothesis, we tested two additional behaviors associated with female internal states. Vaginal plates opening are mostly performed by receptive virgins and very rarely are observed in the early days after copulation (Wang et al., 2021) (Figure 3C). Conversely, mated females reject actively courting males by extruding their ovipositor (Mezzera et al., 2020; Wang et al., 2020a) (Figure 3D). For both of these performances, independent *dsx* heterozygotes also differ from canonical wild-type virgins. Together, *dsx* heterozygosity attenuates virgin behaviors while

enhancing mated-specific PMRs, suggesting subjective induction of the post-mated state (Figures 3A–3D).

Given that female virgin performance depends on *dsx* dosage, we wondered if PMRs in wild-type females could be triggered by a *dsx* decrease as a putative effect of mating. We analyzed Dsx staining in abdominal *SAG-1* neurons, but Dsx levels were similar between virgins and females 24 h post-insemination (Figure 3E). Although this does not preclude that other neuronal lineages might experience Dsx fluctuation, it suggests Dsx is not an active component of the switch.

Expression of Dsx in restricted abdominal neurons is required for virgin behavior

With knowledge that virgin behavior is highly sensitive to *dsx* dosage, we next interrogated where and when Dsx is required in the nervous system for female responses. We used a *dsx-RNAi* stock published by Bruce Baker's lab (*dsx-RNAi[BBJ]*) Robinett et al., 2010) and an independent TRiP-JF line (*dsx-RNAi[JF]*). Although the *dsx-RNAi[BB]* stock actually contains two transgene copies, it was documented to induce only weak *dsx* knockdown at 25°C (Robinett et al., 2010); *dsx-RNAi[JF]* has not been directly assessed for Dsx suppression. We compared their efficacies when activated at 25°C using *SAG-1-Gal4,* which allowed us to quantify Dsx alteration in defined abdominal SAG-1 cells. We found that *dsx-RNAi[BB]* induced mild but significant reduction of Dsx protein, within the range observed in the miRNA and *hth[BSmut]* mutants, while *dsx-RNAi[JF]* caused stronger depletion (Figures 3E and 3F, compare with Figures 2G and 2H). Consistent with this hierarchy, *dsx-RNAi[JF],* but not *dsx-RNAi [BB],* could reduce male sex comb bristles at 25°C (Figure S5). Nevertheless, *dsx-RNAi[JF]* induced only a mild cuticular defect by comparison with the viable *trans*-allelic combination of *dsx [1]/[9],* which yields full loss of differentiated male sex combs (Figure S5), as well as general inter-sex features. Thus, we have inducible genetic reagents that reproduce mild suppression of Dsx protein and function, within a range relevant to disruption of Dsx levels seen in BX-C miRNA and *hth[BSmut]* mutants.

We then used egg-laying and receptivity as readouts to screen a potential shift to a subjective post-mated state. Upon induction of either *dsx-RNAi* transgene with pan-neuronal *elav-Gal4,* both transgenes reliably increased the egg-laying capacity of young virgins (Figure 3G), in line with the results obtained for *dsx* heterozygotes. Similarly, receptivity was significantly compromised (Figure 3H). We additionally tested fertility and climbing in these genetic combinations to rule out general, non-specific effects of *dsx* depletion, undesired side effects of RNAi machinery activation, or possibly off-targeting. Both male and female fertility and locomotion in knockdowns were indistinguishable from controls, emphasizing the specificity of *dsx* function for virgin behaviors, as well as its dose sensitivity compared with cuticular structures, which remain unperturbed under similar *dsx* depletion (Figure S5).

Restricting *dsx* knockdown to specific VT-switch lineages, using *VT-7068* and *VT-50405* Gal4 lines, induced similar effects in both egg-laying and receptivity (Figures 3G and 3H). The effects with *dsx-RNAi[JF]* were stronger than with *dsx-RNAi[BB],* further highlighting the sensitivity of virgin behaviors to *dsx* dosage. Moreover, when *dsx-RNAi* was limited to the intersection of these drivers, the sparser SAG-1 lineage, both RNAi lines induced aberrant egg-laying in young virgins, and *dsx-RNAi[JF]* also substantially compromised

virgin receptivity (Figures 4A and 4B). These phenotypes were in line with those observed in *mir-iab-4/8* and *hth[BSmut]* mutants (Garaulet et al., 2020) (Figures 4A and 4B), suggesting that Dsx decrease may be causal to behavioral defects found in the absence of *hth* regulation by miR-iab-4/8. To investigate if depletion of *dsx* affected neuronal differentiation, we analyzed dendritic (VNC) and axonal (brain) patterns of SAG-1 abdominal neurons in wild-type and both knockdowns. We did not observe any gross anatomical defects upon *dsx* depletion (Figure S5). Altogether, our experiments indicate that virgin behaviors and PMRs are specifically sensitive to Dsx levels. We note that the split-Gal4 system may confer enhanced activity over the individual VT-switch lines. But the fact that the knockdown occurs in very restricted neurons, including the four ascending neurons (Figure 3E), and is only a partial knockdown supports a strong requirement for Dsx in these cells for female behavior.

Having identified a minimal set of neurons where *dsx* is necessary for egg-laying and receptivity, we sought the timing of Dsx activity to regulate these behaviors. Our RNA-seq analysis demonstrates differential expression of *dsx* in miRNA and *hth[BSmut]* mutants in late third instar larvae, prior to the establishment of the adult circuitry controlling PMRs. We temporally restricted *dsx* knockdown by including temperature-sensitive *Gal80* (*tub-Gal80^{ts}*) in *SAG-1>dsx-RNAi[JF]* flies and switching them from the restrictive (18°C) to permissive (29°C) temperatures and vice versa right after at eclosion (Figure 4C). These temperature shifts allowed us to discern between developmental or adult functions of Dsx in SAG-1 neurons in relation to virgin behaviors and PMRs. Monitoring egg-laying and receptivity, we found that adult knockdown induced subtle but statistically significant differences in these two behaviors. Nonetheless, the effects of developmental knockdown were dramatic for virgin performance: while the studied behaviors were unaffected by this temperature regimen in controls (little egg-laying and full receptivity), experimental individuals laid eggs profusely and remained completely refractory to male courtship (Figures 4D and 4E).

Our previous work showed that disruption of miR-iab-4/8 regulation of *hth* in the VNC suppresses virgin behaviors and induces a switch to a subjective mated state (Garaulet et al., 2020). Does depletion of Dsx similarly cause a broad switch in the behavioral output of virgin females toward a subjective mated state? In our Anal tests, we extended our analyses to other behaviors, comparing *SAG-1>dsx-RNAi* with wild-type virgin and mated females, as well as with *mir-iab-4/8* and *hth[BSmut]* mutant virgins. By analyzing other virgin behaviors that are defective in mutants (e.g., opening of vaginal plates), as well as mated behaviors that are ectopically gained by mutant virgins (e.g., ovipositor extrusion), we gain greater confidence that depletion of *dsx* reflects a switch in behavioral state. Indeed, these analyses demonstrate that *SAG-1>dsx-RNAi* females qualitatively fail to coordinate virgin status with virgin behavioral programs and instead act as mated animals (Figures 4A, 4B, 4F, and 4G). For most readouts using *SAG-1 > dsx-RNAi[JF],* the effects observed were also quantitatively comparable with *mir-iab-4/8* deletion and *hth[BSmut]* mutants. Although we do not imply that SAG-1 is the only lineage affected in these mutants, these data reveal that Dsx function in these specific cells is pertinent for normal behavior. In summary, a double-negative regulatory axis within the CNS is critical for virgin females to appropriately coordinate their external behaviors with their internal state (Figure 4H).

DISCUSSION

We recently established how miRNA mediated suppression of the transcription factor Hth to safeguard the virgin female behavioral state (Garaulet et al., 2020). Using engineered alleles and spatio-temporal *hth* manipulations, we demonstrated a developmental requirement for post-transcriptional regulation of Hth within the abdominal ganglion of the CNS for female behavior. However, Hth was not required in otherwise wild-type VT-switch neurons for execution of virgin behaviors, implying that expression of Hth in the abdominal VNC must normally be prevented. This involves integration of two mechanisms: a high density of BX-C miRNA binding sites (miR-iab-4/8) within the *hth-HD* 3′ UTR, as well as neural-specific 3′ UTR elongation, which unveils many of these sites only on neural *hth* isoforms.

Here, we extend this regulatory axis by showing that loss of BX-C miRNAs, acting through derepressed Hth, leads to downregulation of the Dsx in the abdominal VNC. Dsx is well-known as a master sex determination transcription factor (Kopp, 2012), and it shows localized expression in specific CNS domains. However, although the activity of Dsx-expressing neurons per se has been implicated in the switch in females (Feng et al., 2014; Häsemeyer et al., 2009; Yang et al., 2009), the functions of Dsx in post-mitotic neurons are less well defined. Our work reveals that Dsx itself is a central component in specifying virgin behavior, because its restricted suppression in as few as four (SAG-1^{+}) neurons is sufficient to induce post-mated behaviors. It remains to be better defined how SAG-1 neurons are affected by depletion of Dsx. We did not see overt differentiation defects, but we cannot rule out an effect of masculinization. Otherwise, our recent work suggests an activity defect in a general population of switch neurons in the miRNA mutant (Garaulet et al., 2020), but more direct analysis of *dsx*-depleted SAG-1 neurons awaits.

Altogether, in contrast with highly branched regulatory networks that are bioinformatically inferred to lie downstream of individual miRNAs, we reveal a linear, double-negative regulatory cascade comprising miRNAs and two transcription factors (Figure 4H). These findings provide impetus to assess possible direct regulation of Dsx by Hth, as well as to elucidate Dsx targets that are relevant to female behavioral control. Overall, we expand a genetic hierarchy that is essential for females to couple the virgin internal state with appropriate behaviors.

STAR★METHODS

RESOURCE AVAILABILITY

Lead contact—Further information and requests for resources and reagents should be directed to and will be fulfilled by the Lead Contact, Eric Lai (laie@mskcc.org, tel: 212-639-5578).

Materials availability—Transgenic flies generated in this study are available from the corresponding authors on request.

Data and code availability—The original behavior data for Figures 1, 3, 4, and S5 in the paper are available from the corresponding authors. The raw RNA-seq data reported in this

study were deposited in the NCBI Gene Expression Omnibus under accession GEO: GSE166562.

EXPERIMENTAL MODEL AND SUBJECT DETAILS

This study used male and female flies of wild-type and genetically engineered strains of *Drosophila melanogaster.* Virgin and mated parameters refer to assays of female behavioral performances.

Fly strains and maintenance—Larval and adult flies were raised on cornmeal/molasses media recipe: 83.8% water, 0.6% agar, 4.6% cornmeal, 2.3% dried yeast, 7.8% molasses solids, 0.3% propionic acid, 0.1% tegosept, 0.5% ethanol. They were kept at 25°C (unless mentioned otherwise), 55% humidity and under 12h:12h LD cycles.

Drosophila* lines used in this study—mir[Δ]* (Bender, 2008), *mir* [*C11*] and *hth[BSmut]* (Garaulet et al., 2020), *Canton-S* (gift of Karla Kaun), *VT-lines* and *SAG-1* split Gal4 line (Feng et al., 2014), *UAS-hth-RNAi* (Vienna *Drosophila* RNAi Center), *2xUAS-dsx-RNAi[BB]* (Robinett et al., 2010), *tub-GFP-mir-iab-4 and -iab-8* sensors (Tyler et al., 2008). The following lines were obtained from Bloomington *Drosophila* Stock Center: *elav-Gal4 [C-155]* (BDSC #458), *UAS-mCD8-GFP* (BDSC #5137), *UAS-Red-Stinger* (BDSC #8547), *tubGal80^{ts}* (BDSC #7108), *UAS-dsx-RNAi [JF]* (BDSC #26716), *dsx[1]* (BDSC #1679), *dsx[9]* (BDSC #44223), *UAS-dsxF* (BDSC #44223).

All the lines used in this study have been backcrossed at least 8 generations to the *Canton-S* wild-type strain.

METHOD DETAILS

RNA extraction and sequencing—Female larvae were dissected on ice for a maximum of 30 minutes (30-40 larvae). The posterior third of larvae was removed with forceps, the remaining was turned inside down. Using 2mm curved blade spring scissors (Fine Science Tools #15000-04), VNC were severed at the level of the A7 pair of nerves, and immediately placed into TRIzol (Thermo Fisher Scientific #15596018). After dissections, samples in TRIzol were stored at −80°C. Each biological replicate pooled severed VNCs of 120-150 larvae, dissected in 4-5 periods of 30 min. 3 replicates were generated per genotype. RNA extraction was performed with TRIzol.

500 ng of total RNA per dissected VNC sample was used for TruSeq stranded mRNA library preparation (Illumina) by the Integrated Genomics Operation (IGO) core at MSKCC. Libraries were sequenced on Illumina HiSeq-1000 sequencer with PE-100 mode. The raw sequence data are available from GEO accession number: GEO: GSE.166562.

Bioinformatic analysis—RNA-seq data were aligned to the *Drosophila melanogaster* reference genome (Version r6.21) using HISAT2 software with standard parameters (Kim et al., 2015). We used featureCounts in the Rsubread package to compute features and read numbers for each bam file (Liao et al., 2019). The read counts per gene were then normalized to obtain RPKM values using edgeR package from R Bioconductor (Robinson et al., 2010) and extracting transcript length from Biomart (Durinck et al., 2005). Fold changes

between samples were calculated using edgeR applying no filter. Genes targeted by miR-iab-8-5p were identified using conserved TargetScanFly predictions (Agarwal et al., 2018).

Immunohistochemistry, imaging, and image quantification analysis—Larval and adult CNS were dissected in cold PBS and fixed for 1h in 4% paraformaldehyde + 0.1% Triton. Primary and secondary antibodies were incubated for > 36h at 4°C in wash buffer (PBS +1% BSA) and mounted in Vectashield (Vector Labs). Antibodies used were mouse anti-abd-A (gift of Ian Duncan), rabbit and guinea pig anti-Hth (Salvany et al., 2009), rat anti-Dsx (Sanders and Arbeitman, 2008) and Alexa- 488, –555, –647 conjugated goat and/or donkey antibodies from Thermo Fisher Scientific.

Imaging was performed in a Leica TCS SP5 confocal microscope. Each VNC was typically scanned in 55 planes (Z step ~2 μm). When image quantification or comparison was performed (Figures 2 and 3), all different genotypes used were dissected at the same time, fixed and incubated together in the same well. To identify the genotype of each VNC while mounting, different parts of the head (eyes, proboscis, antennae, etc.) were left attached or removed from the VNC during dissection. Then, the same number of VNCs from different genotypes were arranged in a known fashion per slide, to avoid differences in the quantification due to the mounting process. Laser power and offset were maintained identically for all the samples being compared. Gain was slightly adjusted to an internal control in each case.

Image quantification analysis was performed using FIJI (Schindelin et al., 2012). To obtain the values of Dsx intensity, each nuclei was identified on the GFP channel, its Dsx/Hth signal measured, and individually normalized by subtracting the background signal of a similar area in the cytoplasmic region of the same cell. All adult VNC images are 0-24 hr old females.

Behavioral assays—We collected virgin males and females after eclosion and kept them isolated in vials at 25°C, 55% humidity and 12h:12h LD cycles until utilized for behavior assays. All tests were performed at ZT 7-11 and at least at four different occasions. Vaginal plate opening, ovipositor extrusions and receptivity were assayed at day 3 after eclosion in custom 18-multiplex mating arenas (chamber size: 10 mm diameter). From eclosion to day 3, individual male and female virgins were kept isolated in vials. At day 3, single males and females were placed in a half of each arena and allowed to acclimate for 5 min before the assay. Then, they were allowed to interact and recorded for 10 minutes. Ovipositor extrusions and vaginal plates openings were analyzed during the first 4 minutes after courtship initiation or until mating. Counts of either behavior were normalized to time (min). Receptivity was calculated as the cumulative proportion of animals mated at 10 min. Egg-laying was calculated as the number of eggs laid in the first 3 days after eclosion (for virgins of all genotypes), and during the first 24h after copulation (for mated females).

For mated behaviors, virgin females were kept isolated in individual vials. At day 3, they were allowed to mate to CS males, and immediately separated from males after copulation. Then, they were placed individually in single vials. Egg-laying in mated females is the number of eggs laid per female during the first 24h after mating. At 24h after mating, mated

females were assayed for vaginal plate opening, ovipositor extrusions and receptivity with fresh males, following the protocol detailed above.

For temperature shifts, flies carrying *tub-Gal80^{ts}* were placed at either restrictive (18°C) or permissive (29°C) temperature during development, and shifted to the new temperature immediately after eclosion. 55% humidity and 12h:12h LD cycles were maintained.

Negative geotaxis was estimated in male flies as the average time required to climb a height of 9 cm inside a fly vial. Flies were house kept in vials in groups of as many as 5 flies right after eclosion. After 3-5 days, wings were manually clipped under CO2 flow, and returned to the vial for additional 48h. Then, they were transferred to an experimental vial with no food and recorded for 2-3 minutes after 3 taps. Each fly was monitored for three trials.

Fertility was measured as the proportion of flies giving rise to viable progeny. Individual males and females were crossed to 3 flies of the opposite sex in single vials. Progeny was screened in these vials one week after.

QUANTIFICATION AND STATISTICAL ANALYSIS

Statistical significance was evaluated using Fisher's exact test for receptivity (Figures 3 and 4) and fertility (Figure S5); Mann-Whitney non parametric test for egg-laying (Figures 3 and 4), ovipositor extrusions (Figures 3 and 4), vaginal plates openings (Figures 3 and 4), fluorescence intensity (Figures 2 and 3; Figure S4), number of nuclei (Figure 1), number of sex combs (Figure S5), and climbing (Figure S5); and unpaired t test with Welch's correction for differential gene expression analysis (Figures 1 and 2) and number of neurons (Figure 2). Ns = not significant, * $p < 0.05$, ** $p < 0.01$, *** $p < 0.001$, **** $p < 0.0001$. Error bars in Figures 1, 2, 3, 4, and S5 represent SEM. All n values are displayed on the figures.

Supplementary Material

Refer to Web version on PubMed Central for supplementary material.

ACKNOWLEDGMENTS

We thank Welcome Bender, Barry Dickson, Natalia Azpiazu, Carlos Ribeiro, Carolina Rezaval, Stephen Goodwin, Karla Kaun, Michelle Arbeitman, Richard Mann, Ian Duncan, and the Bloomington *Drosophila* Stock Center for fly strains, plasmids, and antibodies used in this study. We thank Ernesto Sánchez-Herrero and Paloma Martín for help and support. Work in E.C.L.'s group was supported by the NIH (R01-GM083300 and R01-NS083833) and MSK Core grant P30-CA008748.

REFERENCES

Agarwal V, Subtelny AO, Thiru P, Ulitsky I, and Bartel DP (2018). Predicting microRNA targeting efficacy in Drosophila. Genome Biol. 19, 152. [PubMed: 30286781]

Anholt RRH, O'Grady P, Wolfner MF, and Harbison ST (2020). Evolution of Reproductive Behavior. Genetics 214, 49–73. [PubMed: 31907301]

Bender W (2008). MicroRNAs in the Drosophila bithorax complex. Genes Dev. 22, 14–19. [PubMed: 18172161]

Casares F, and Mann RS (1998). Control of antennal versus leg development in Drosophila. Nature 392, 723–726. [PubMed: 9565034]

Durinck S, Moreau Y, Kasprzyk A, Davis S, De Moor B, Brazma A, and Huber W (2005). BioMart and Bioconductor: a powerful link between biological databases and microarray data analysis. Bioinformatics 21, 3439–3440. [PubMed: 16082012]

Feng K, Palfreyman MT, Häsemeyer M, Talsma A, and Dickson BJ (2014). Ascending SAG neurons control sexual receptivity of Drosophila females. Neuron 83, 135–148. [PubMed: 24991958]

Garaulet DL, Castellanos MC, Bejarano F, Sanfilippo P, Tyler DM, Allan DW, Sánchez-Herrero E, and Lai EC (2014). Homeotic function of Drosophila Bithorax-complex miRNAs mediates fertility by restricting multiple Hox genes and TALE cofactors in the CNS. Dev. Cell 29, 635–648. [PubMed: 24909902]

Garaulet DL, Zhang B, Wei L, Li E, and Lai EC (2020). miRNAs and Neural Alternative Polyadenylation Specify the Virgin Behavioral State. Dev. Cell 54, 410–423.e4. [PubMed: 32579967]

Gummalla M, Maeda RK, Castro Alvarez JJ, Gyurkovics H, Singari S, Edwards KA, Karch F, and Bender W (2012). abd-A regulation by the iab-8 noncoding RNA. PLoS Genet. 8, e1002720. [PubMed: 22654672]

Häsemeyer M, Yapici N, Heberlein U, and Dickson BJ (2009). Sensory neurons in the Drosophila genital tract regulate female reproductive behavior. Neuron 61, 511–518. [PubMed: 19249272]

Jang YH, Chae HS, and Kim YJ (2017). Female-specific myoinhibitory peptide neurons regulate mating receptivity in Drosophila melanogaster. Nat. Commun 8, 1630. [PubMed: 29158481]

Kim D, Langmead B, and Salzberg SL (2015). HISAT: a fast spliced aligner with low memory requirements. Nat. Methods 12, 357–360. [PubMed: 25751142]

Kopp A (2012). Dmrt genes in the development and evolution of sexual dimorphism. Trends Genet. 28, 175–184. [PubMed: 22425532]

Kubli E, and Bopp D (2012). Sexual behavior: how Sex Peptide flips the postmating switch of female flies. Curr. Biol 22, R520–R522. [PubMed: 22789998]

Liao Y, Smyth GK, and Shi W (2019). The R package Rsubread is easier, faster, cheaper and better for alignment and quantification of RNA sequencing reads. Nucleic Acids Res. 47, e47. [PubMed: 30783653]

McRobert SP, and Tompkins L (1985). The effect of transformer, doublesex and intersex mutations on the sexual behavior of Drosophila melanogaster. Genetics 111, 89–96. [PubMed: 3928434]

Mezzera C, Brotas M, Gaspar M, Pavlou HJ, Goodwin SF, and Vasconcelos ML (2020). Ovipositor Extrusion Promotes the Transition from Courtship to Copulation and Signals Female Acceptance in Drosophila melanogaster. Curr. Biol 30, 3736–3748.e5. [PubMed: 32795437]

Nothiger R, Leuthold M, Andersen N, Gerschwiler P, Grüter A, Keller W, Leist C, Roost M, and Schmid H (2009). Genetic and developmental analysis of the sex-determining gene ‘double sex’ (dsx) of Drosophila melanogaster. Genet. Res 50, 113–123.

Ogawa S, and Makino J (1984). Aggressive behavior in inbred strains of mice during pregnancy. Behav. Neural Biol 40, 195–204. [PubMed: 6539590]

Pai CY, Kuo TS, Jaw TJ, Kurant E, Chen CT, Bessarab DA, Salzberg A, and Sun YH (1998). The Homothorax homeoprotein activates the nuclear localization of another homeoprotein, extradenticle, and suppresses eye development in Drosophila. Genes Dev. 12, 435–446. [PubMed: 9450936]

Rezával C, Pavlou HJ, Dornan AJ, Chan YB, Kravitz EA, and Goodwin SF (2012). Neural circuitry underlying Drosophila female postmating behavioral responses. Curr. Biol 22, 1155–1165. [PubMed: 22658598]

Rideout EJ, Dornan AJ, Neville MC, Eadie S, and Goodwin SF (2010). Control of sexual differentiation and behavior by the doublesex gene in Drosophila melanogaster. Nat. Neurosci 13, 458–466. [PubMed: 20305646]

Rieckhof GE, Casares F, Ryoo HD, Abu-Shaar M, and Mann RS (1997). Nuclear translocation of extradenticle requires homothorax, which encodes an extradenticle-related homeodomain protein. Cell 91, 171–183. [PubMed: 9346235]

Robinett CC, Vaughan AG, Knapp JM, and Baker BS (2010). Sex and the single cell. II. There is a time and place for sex. PLoS Biol. 8, e1000365. [PubMed: 20454565]

Robinson MD, McCarthy DJ, and Smyth GK (2010). edgeR: a Bioconductor package for differential expression analysis of digital gene expression data. Bioinformatics 26, 139–140. [PubMed: 19910308]

Salvany L, Aldaz S, Corsetti E, and Azpiazu N (2009). A new role for hth in the early pre-blastodermic divisions in Drosophila. Cell Cycle 8, 2748–2755. [PubMed: 19652544]

Sanders LE, and Arbeitman MN (2008). Doublesex establishes sexual dimorphism in the Drosophila central nervous system in an isoform-dependent manner by directing cell number. Dev. Biol 320, 378–390. [PubMed: 18599032]

Schindelin J, Arganda-Carreras I, Frise E, Kaynig V, Longair M, Pietzsch T, Preibisch S, Rueden C, Saalfeld S, Schmid B, et al. (2012). Fiji: an open-source platform for biological-image analysis. Nat. Methods 9, 676–682. [PubMed: 22743772]

Soller M, Haussmann IU, Hollmann M, Choffat Y, White K, Kubli E, and Schäfer MA (2006). Sex-peptide-regulated female sexual behavior requires a subset of ascending ventral nerve cord neurons. Curr. Biol 16, 1771–1782. [PubMed: 16979554]

Svare B, Mann MA, Broida J, and Michael SD (1982). Maternal aggression exhibited by hypophysectomized parturient mice. Horm. Behav 16, 455–461. [PubMed: 6891694]

Tyler DM, Okamura K, Chung WJ, Hagen JW, Berezikov E, Hannon GJ, and Lai EC (2008). Functionally distinct regulatory RNAs generated by bidirectional transcription and processing of microRNA loci. Genes Dev. 22, 26–36. [PubMed: 18172163]

Wang F, Wang K, Forknall N, Parekh R, and Dickson BJ (2020a). Circuit and Behavioral Mechanisms of Sexual Rejection by Drosophila Females. Curr. Biol 30, 3749–3760.e3. [PubMed: 32795445]

Wang F, Wang K, Forknall N, Patrick C, Yang T, Parekh R, Bock D, and Dickson BJ (2020b). Neural circuitry linking mating and egg laying in Drosophila females. Nature 579, 101–105. [PubMed: 32103180]

Wang K, Wang F, Forknall N, Yang T, Patrick C, Parekh R, and Dickson BJ (2021). Neural circuit mechanisms of sexual receptivity in Drosophila females. Nature 589, 577–581. [PubMed: 33239786]

Yang CH, Rumpf S Xiang Y, Gordon MD, Song W, Jan LY, and Jan YN (2009). Control of the postmating behavioral switch in Drosophila females by internal sensory neurons. Neuron 61, 519–526. [PubMed: 19249273]

Highlights

- RNA-seq analysis reveals genes downstream of miR-iab-4/8/*homothorax* regulon
- miR-iab-4/8 regulation of *homothorax* determines Doublesex levels in *Drosophila* female CNS
- Developmental control of miR/Hth/Dsx circuit regulates female behavior

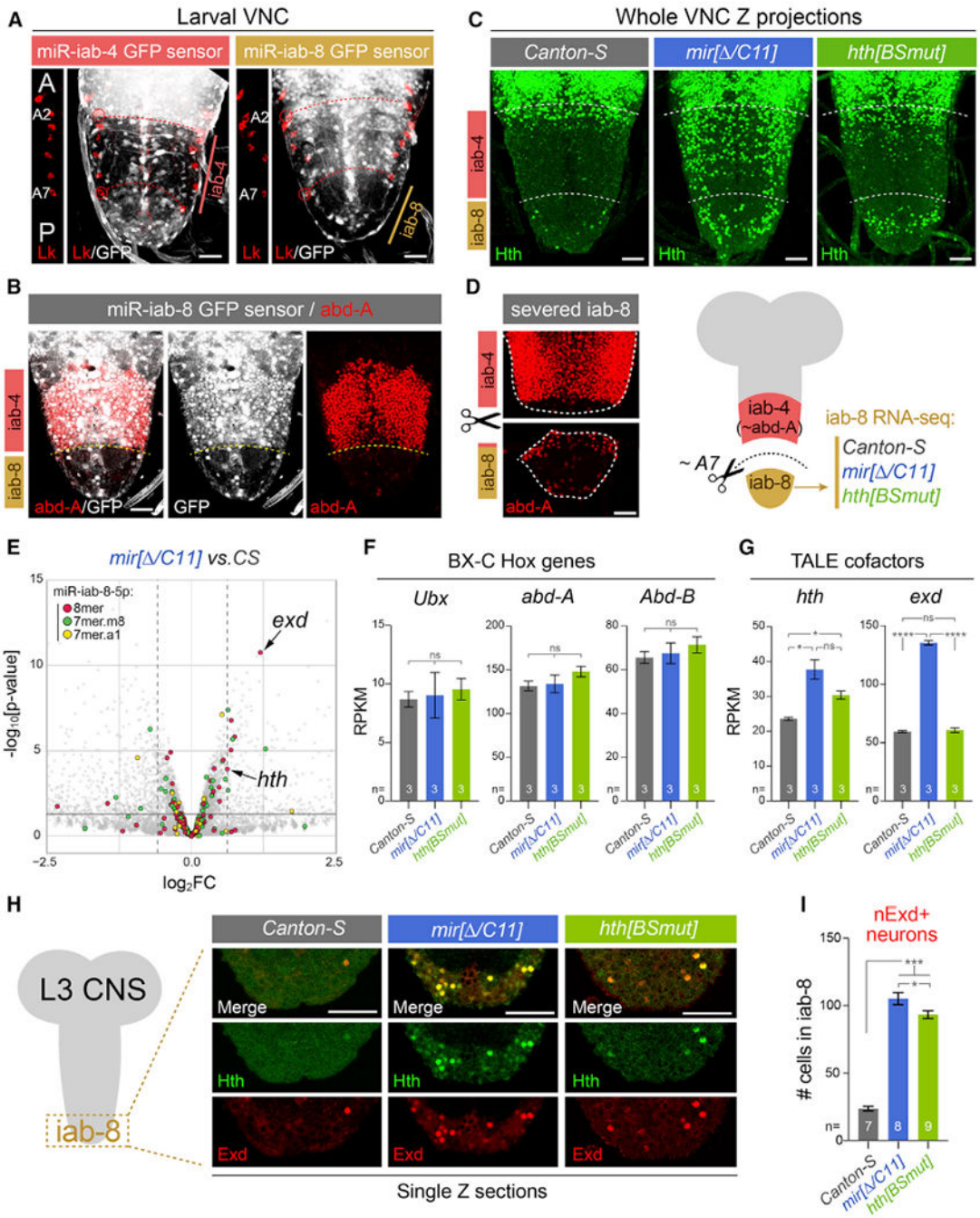

Figure 1. Cytological and transcriptomic analysis of a key miRNA/target regulon in the larval ventral nerve cord (VNC)

All stainings depict third instar larval VNC.

(A) The Bithorax Complex (BX-C) miRNA locus yields *mir-iab-4* and *mir-iab-8* from opposite strands. Their activity is associated with repression of ubiquitously transcribed tub-GFP-miRNA sensors, revealing distinct domains in abdominal segments, whose registers are marked by segmental marker Leukokinin (Lk; red).This places miR-iab-4-5p activity in segments A2–A7 and miR-iab-8-5p in A8–A9. A portion of the Lk staining is shown to the left of each image to reference the segment locations.

(B) The posterior limit of abd-A (A7a/p) corresponds to the miR-iab-4/miR-iab-8 border.
(C) Homothorax (Hth) is largely absent throughout the abdominal VNC in wild-type flies but is derepressed in *mir-iab-4/8* and *hth[BSmut]* mutants, most overt within the iab-8 domain.
(D) Validation of dissection strategy to prospectively isolate A8–A9 VNC domain (iab-8 region) for transcriptomics. Stainings show two pieces of an individual VNC, which were imaged separately for this montage.
(E) Volcano plot of transcripts >1 reads per kilobase of transcript, per million mapped reads (RPKM) showing that TALE cofactors *hth* and *exd* are among the most significantly derepressed miR-iab-8-5p targets in the BX-C miRNA mutant VNC; most other direct targets were unaffected. Black horizontal line demarcates the 0.05 cutoff for p value; dotted vertical lines indicate the 1.5 cutoff for fold change.
(F and G) Comparison of BX-C Hox genes and TALE cofactors expression in wild-type, miRNA mutant, and *hth[BSmut]* iab-8 domain VNCs. *exd* is derepressed in the miRNA mutant, but not in *hth[BSmut]*.
(H) Single-plane confocal images demonstrating nuclear colocalization of Hth and Exd in the iab-8 domain of *mir-iab-4/8* and *hth[BSmut]* VNCs.
(I) Quantification of ectopic nuclear Exd cells in the iab-8 domain of VNCs of the indicated genotypes.
Statistical significance was evaluated using unpaired t test with Welch's correction (F and G) and Mann-Whitney non-parametric test (I). Three biological replicates per genotype were used for transcriptome analysis shown in (E)–(G). *$p < 0.05$, ***$p < 0.001$, ****$p < 0.0001$; ns, not significant. Error bars, SEM. Scale bars, 25 μm (A–D); 40 μm (H). A, anterior; p, posterior.

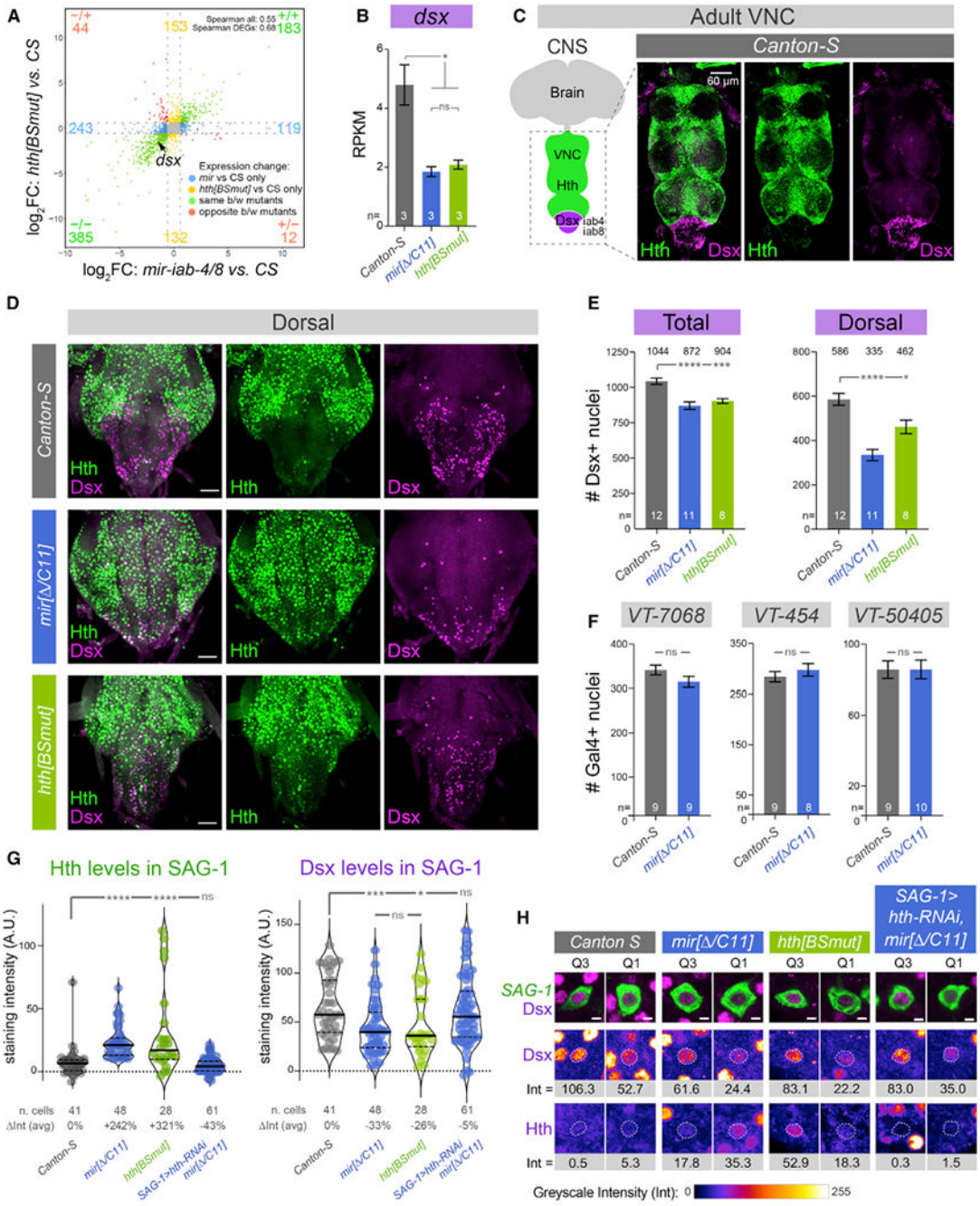

Figure 2. A double-negative gene-regulatory circuit: BX-C miRNAs prevent Hth from excluding Dsx in the VNC

(A) Transcriptome analysis reveals substantial similarity in the larval iab-8 domain of the BX-C miRNA and *hth[BSmut]* mutants, compared with *Canton-S* (three biological replicates per genotype). Only genes > 1 RPKM and $p < 0.05$ are plotted. Dotted gray lines indicate fold change = 1.5.

(B) A notable downregulated transcript in both mutants is the sex-specific differentiation factor *doublesex* (*dsx*).

(C) Hth and Dsx proteins are spatially complementary in the adult VNC.

(D) Derepression of Hth in BX-C miRNA mutant (*mir[Δ/C11]*) and *hth[BSmut]* compromises accumulation of Dsx in abdominal segments of adult VNCs, especially in dorsal planes as shown here.

(E) Quantification of Dsx^+ nuclei in wild-type, BX-C miRNA mutant, and *hth[BSmut]* VNC; total VNC and dorsal half are shown. The number of Dsx+ neurons is compromised in the mutant conditions.

(F) Conversely, the number of other identified abdominal subpopulations that mediate PMRs (VT-switch lines) are not affected by miRNA deletion.

(G) Quantification of Hth and Dsx protein levels in individual abdominal neurons relevant to the female post-mating switch (abdominal SAG-1 neurons). Depression of Hth correlates with reduction of Dsx within identified neurons.

(H) Representative GFP-labeled SAG-1 neurons from higher (Q3) and lower (Q1) quartiles of Dsx, as quantified in (G), with corresponding Dsx and Hth levels. The nuclear levels of each factor (Int) were calculated by subtracting the signals in cytoplasm (marked in green) from the corresponding nucleus (dotted line) for each antigen; samples were co-stained and imaged in parallel within the linear range.

t test with Welch's correction (B, E, and F); Mann-Whitney non-parametric test (G). *$p < 0.05$, ***$p < 0.001$, ****$p < 0.0001$; ns, not significant. Error bars, SEM. Scale bars, 60 μm (C); 30 μm (D); 2 μm (H).

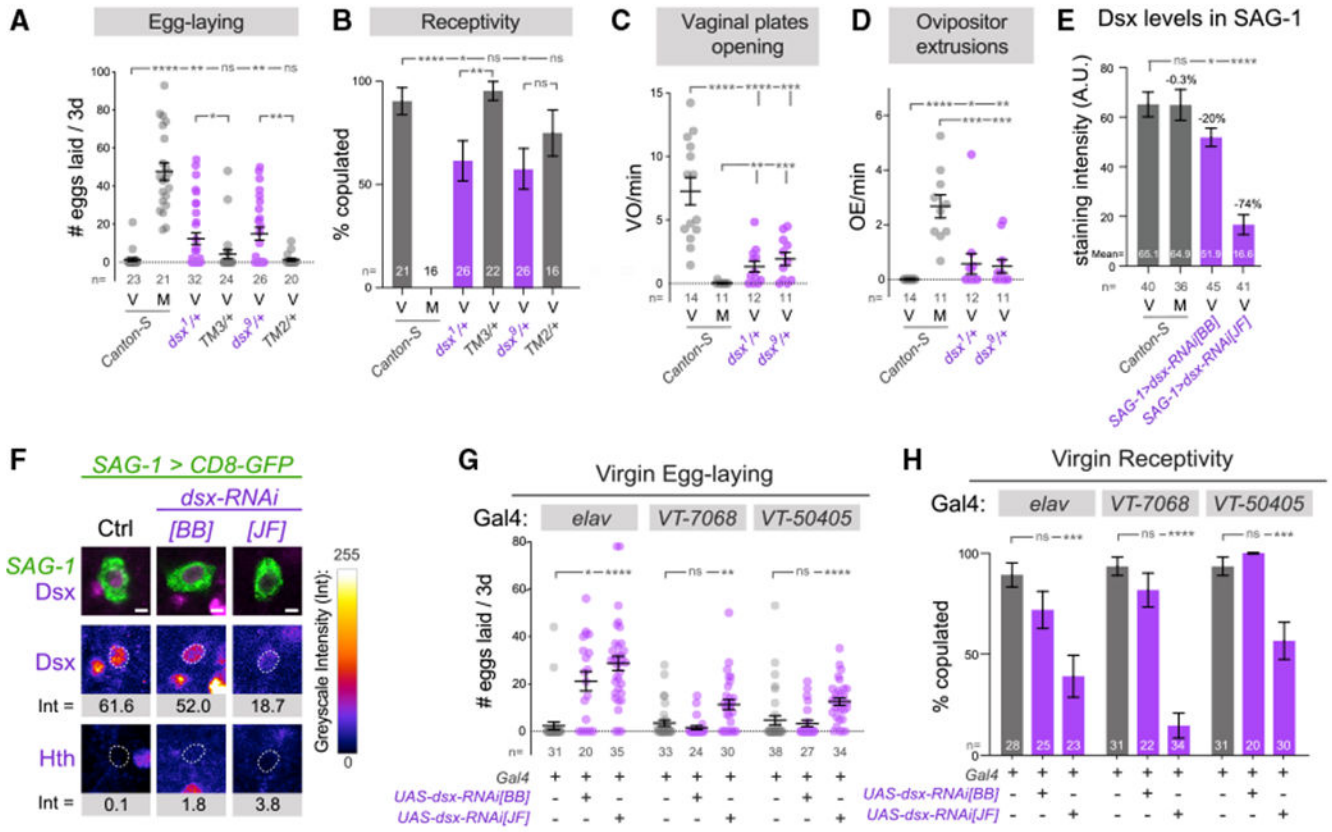

Figure 3. Endogenous Dsx is essential for females to interpret the virgin behavioral state

(A–D) Comparison of female behaviors in wild-type virgins, mated females, and *doublesex* heterozygotes, illustrating a partial transition to the mated state in the latter.

(E) Analysis of Dsx levels in abdominal SAG-1 neurons pre- and 24 h post-insemination and in virgins using independent *dsx-RNAi* transgenes. *dsx-RNAi[JF]* has a stronger effect on Dsx in SAG-1 neurons.

(F) Representative GFP-labeled abdominal SAG-1 neurons from average Dsx levels are shown, with corresponding Dsx and Hth staining. The dotted line corresponds to the nucleus of each neuron.

(G and H) Pan-neuronal knockdown of *dsx* results in increased egg-laying and decreased receptivity by female virgins. Restricted knockdown using VT-switch lines and *dsx-RNAi[JF]* transgene also induces virgin egg-laying and reduces receptivity.

Mann-Whitney non-parametric test (A, C–E, and G); Fisher's exact test (B and H). *p < 0.05, **p < 0.01, ***p < 0.001, ****p < 0.0001; ns, not significant. Error bars, SEM. Scale bar, 2 μm (F). Eggs were collected over 3 days for all virgin genotypes and over the first 24 h after copulation in mated flies (A and G). M, mated females; V, virgin females.

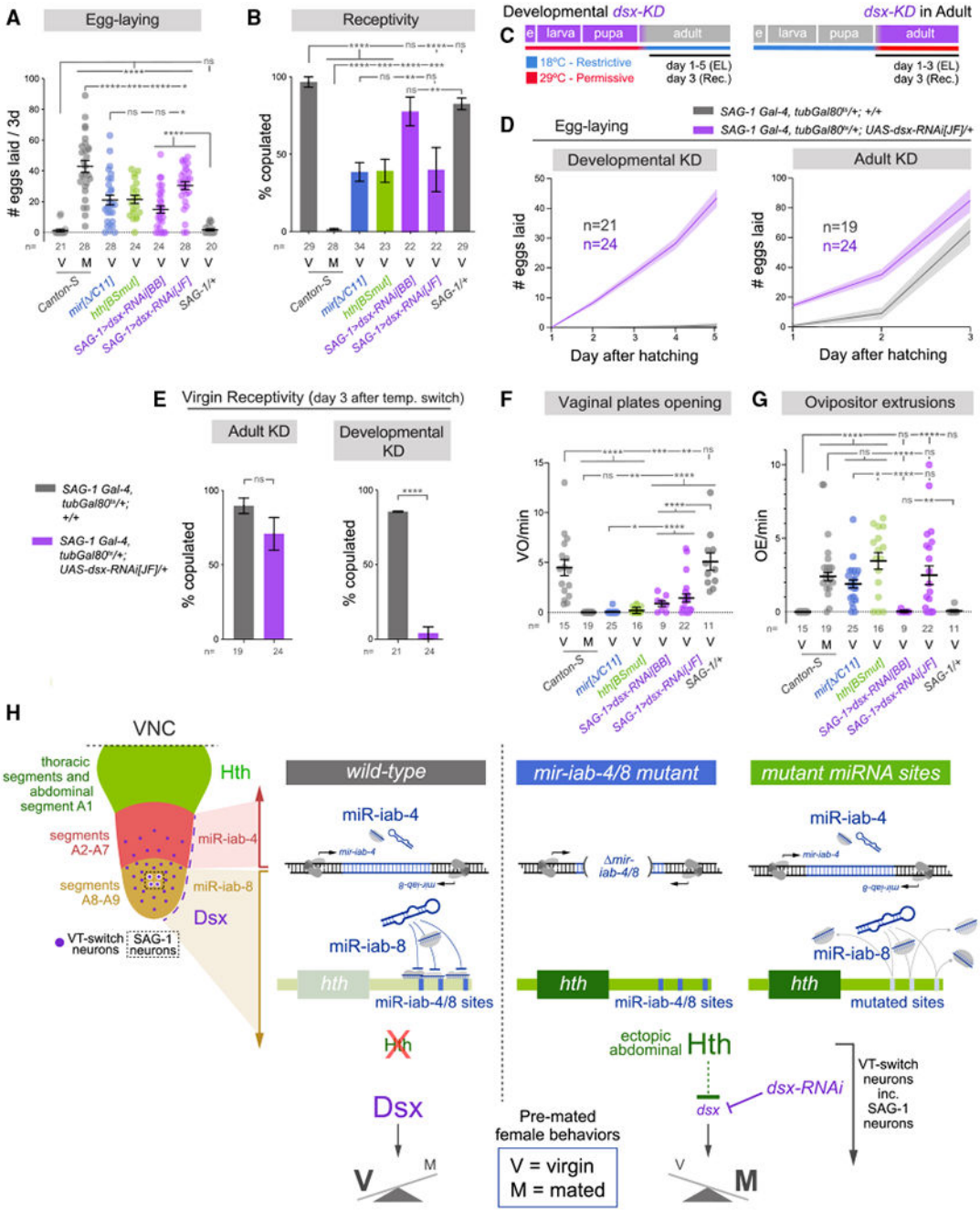

Figure 4. SAG-1 neurons specifically require Dsx for a suite of female virgin behaviors

(A and B) Suppression of Dsx within the SAG-1 lineage enhances egg-laying and compromises virgin receptivity, similar to whole-animal *mir-iab-4/8* deletion and *hth[BSmut]* mutants. *dsx-RNAi[JF]* has a stronger effect.

(C) Strategy for temporal depletion of *dsx*. EL, egg-laying; Rec., receptivity.

(D and E) Analysis of egg-laying (D) and receptivity (E) in flies with developmental or adult knockdown of *dsx*, highlighting the developmental role of *dsx* for virgin adult behaviors.

(F and G) Modulation of Dsx levels also decreases vaginal plates opening (F) and induces ovipositor extrusions (G), comparable with *mir-iab-4/8* deletion and *hth [BSmut]* mutants. (H) Model for the genetic and spatial control of female virgin behavior in the VNC. Upper left, larval VNC illustrates the protein domains of Hth (in thoracic segments and A1) and Dsx (in A2–A9), and RNA domains of *mir-iab-4* (A2–A7) and *mir-iab-8* (A8–A9). Restricted neural populations that govern the female post-mating switch are distributed within A2–A9 (VT-switch neurons), including four SAG-1 neurons within the *mir-iab-8* domain. In wild-type abdominal VNC, the activity of *mir-iab-4/8* binding sites on *hth-3*0 *UTR*, or depleted of *dsx* within VT-switch neurons (and in as few as those of highly restricted SAG-1 neurons) exhibit a switch from virgin to post-mated behaviors. Mann-Whitney non-parametric test (A, F, and G); Fisher's exact test (B and E). *$p < 0.05$, **$p < 0.01$, ***$p < 0.001$, ****$p < 0.0001$; ns, not significant. Error bars, SEM. Eggs were collected over 3 days for all virgin genotypes and over the first 24 h after copulation in mated flies. V, virgin; M, mated.

KEY RESOURCES TABLE

REAGENT or RESOURCE	SOURCE	IDENTIFIER
Antibodies		
rabbit anti-Hth (1:500)	Salvany et al., 2009	N/A
guinea pig anti-Hth (1:500)	Salvany et al., 2009	N/A
Mouse anti-Abd-A (1:500)	Gift of Ian Duncan	Department of Biology. Washington University in St. Louis
Rat anti-Dsx	Sanders and Arbeitman, 2008	RRID: AB_2569439
Donkey anti-rabbit Alexa fluor 488	Thermo Fisher Scientific	Cat# A32790; RRID: AB_2762833
Goat anti-rabbit Alexa fluor 647	Thermo Fisher Scientific	Cat# A32733; RRID: AB_2633282
Donkey anti-mouse Alexa fluor 594	Thermo Fisher Scientific	Cat# A32744; RRID: AB_2762826
Donkey anti-mouse Alexa fluor 647	Thermo Fisher Scientific	Cat# A32787; RRID: AB_2762830
Goat anti-guinea pig Alexa fluor 488	Thermo Fisher Scientific	Cat# A-11073; RRID: AB_2534117
Donkey anti-rat Alexa fluor 594	Thermo Fisher Scientific	Cat# A-21209; RRID: AB_2535795
Chemicals, peptides, and recombinant proteins		
Gel Loading Buffer II	Invitrogen	AM8547
AccuPrime Pfx DNA Polymerase	Thermo Fisher	12344024
Trizol reagent	Life Technologies	15596018
Oligo d(T)25 Magnetic Beads	New England Biolabs	S1419S
Millennium RNA Markers	Thermo Fisher	AM7150
Amersham Megaprime DNA Labeling System	Cytiva	RPN1606
VECTASHIELD_ Vibrance Antifade Mounting Medium without DAPI	Vector Laboratories	H-1700-2
VECTASHIELD_ Antifade Mounting Medium with DAPI	Vector Laboratories	H-1500-10
Experimental models: Organisms/Strains		
mir[C11]	Garaulet et al., 2020, Eric Lai lab.	N/A
mir[Δ]	Bender, 2008, Gift of Welcome Bender, Harvard University	N/A
Canton-S	Gift of Karla Kaun, Department of Neuroscience, Brown University.	N/A
VT-lines and SAG-1 split Gal4 line	Feng et al., 2014, Gift of Barry Dickson, Janelia Farm Research Campus.	N/A
tub-GFP-sensors for miR-iab-4 and miR-iab-8	Tyler et al., 2008, Eric Lai lab	N/A
hth[BSmut]	Garaulet et al., 2020, Eric Lai lab.	N/A
2xUAS-dsx-RNAi[BB]	Robinett et al., 2010	N/A
UAS-hth-RNAi	Vienna Drosophila RNAi Center	100630
tubGal80^{ts}	Bloomington Drosophila Stock Center	7108
elav-Gal4[C-155]	Bloomington Drosophila Stock Center	458
UAS-mCD8-GFP	Bloomington Drosophila Stock Center	5137
UAS-Red-Stinger	Bloomington Drosophila Stock Center	8547
UAS-dsx-RNAi[JF]	Bloomington Drosophila Stock Center	26716

REAGENT or RESOURCE	SOURCE	IDENTIFIER
dsx[1]	Bloomington Drosophila Stock Center	1679
dsx[9]	Bloomington Drosophila Stock Center	44223
UAS-dsxF	Bloomington Drosophila Stock Center	44223
UAS-hth	Gift of Richard S. Mann, Columbia University. Casares and Mann, 1998	N/A
Deposited data		
VNC RNA-seq data	This study.	NCBI GEO: GSE166562
Software and algorithms		
Prism 7 for Mac OS X	GraphPad	https://www.graphpad.com
Fiji ImageJ 2.0.0-rc-68/1.52e	N/A	https://imagej.nih.gov/ij
Rstudio Version 1.2.1335	Rstudio	https://www.rstudio.com/
IGV_2.6.3	Broad Institute	http://software.broadinstitute.org/software/igv/